Bidirectional changes in postmitotic H3K27me3 distributions underlie cerebellar granule neuron maturation dynamics

Vijyendra Ramesh[1,2], Fang Liu[1,3], Melyssa S. Minto[3], Urann Chan[3] and Anne E. West[2,3]

[1]These authors contributed equally

[2]Molecular Cancer Biology Program, Duke University School of Medicine, Durham, NC-27705

[3]Department of Neurobiology, Duke University School of Medicine, Durham, NC-27705

Abstract

The functional and transcriptional maturation of neurons is a prolonged process that extends well beyond mitotic exit and terminal fate commitment of progenitors. The differentiation of cerebellar granule neurons (CGNs) in the postnatal mouse cerebellum provides a useful model to identify chromatin mechanisms that orchestrate temporal changes in transcription as postmitotic CGNs mature. Here we report that CGN maturation is associated with dynamic changes in the genomic distribution of histone H3 lysine 27 trimethylation (H3K27me3), a modification best known for its role in repressing alternative fates during cell specification. H3K27me3 is gained rapidly in newly postmitotic CGNs at progenitor-expressed genes that are repressed in neurons. H3K27me3 is lost more gradually at the promoters of a subset of neuronal genes that are transcriptionally induced upon CGN maturation. The loss of H3K27me3 is facilitated by the lysine demethylase KDM6B, and genes that are induced in maturing CGNs show impaired expression in the cerebellum of conditional KDM6B knockout mice. Genes that lose H3K27me3 gain H3K27 acetylation and binding of the pro-maturation ZIC1/2 transcription factors, suggesting that developmental loss of H3K27me3 may be required to permit the onset of transcriptional maturation. Interestingly, pharmacological inhibition of the H3K27 methyltransferase EZH2 in early postmitotic CGNs not only blocked the repression of progenitor genes but also impaired the induction of mature CGN genes. These data show that regulation of H3K27me3 functions in developing postmitotic neurons beyond the period of cell fate commitment to regulate the dynamics of gene expression programs that underlie functional neuronal maturation.

Introduction

Cell identity is determined during differentiation by the coordinated actions of chromatin regulatory factors, which serve to establish the accessibility of gene regulatory elements that control transcription of cell-type specific genes. Histone proteins play a key role in determining the architecture of chromatin, and specific post-translational modifications of the histones are tightly associated with the transcriptional state of a given locus or gene [1]. Among these modifications, histone methylation occurs on lysine and arginine residues of specific histones, and has roles in both gene activation and repression [2], and acts to alter gene transcription by recruiting the site-specific binding of effector proteins that carry out specialized functions [3]. The trimethylation of lysine 27 on histone H3 (H3K27me3) is a repressive histone modification that is best known for its role during cell-fate determination [4]. H3K27 methylation is deposited by the Polycomb repressive complex 2 (PRC2) lysine methyltransferases EZH1 and EZH2 [5, 6]. H3K27me3 can be enzymatically removed by the H3K27-specific lysine demethylases KDM6A (UTX) and KDM6B (JMJD3) [7]. In mice, null mutations in *Ezh2* result in early embryonic lethality [5] and *Kdm6a* knockouts show severely impaired mid-gestational development [8], suggesting the physiological importance of H3K27me3 regulation for mammalian embryonic development.

At the cellular level, the functions of H3K27me3-dependent gene regulation in cell fate determination are well established [9]. In stem cells, the colocalization of H3K27me3 with the active histone marks H3K4me3 and H3K27ac at regulatory elements of cell-type specific genes is thought to poise these genes for subsequent activation or silencing upon terminal differentiation depending on the chosen fate of the cell. Activation of poised genes that function in the chosen fate is associated with the permanent loss of H3K27me3, whereas persistent silencing of genes that define alternative fates is mediated by recruitment of the PRC1 complex. Interestingly, the enzymes that regulate H3K27me3 remain expressed in fate-committed, postmitotic neurons both during postnatal stages of development and in the adult brain [10, 11], where their functions are less well understood. Genetic evidence that ongoing regulation of H3K27me3 after fate commitment might be important emerged when conditional

76 deletion of both *Ezh1* and *Ezh2* in neurons of the adult mouse striatum was shown to cause a
77 slow global loss of H3K27me3 as well as progressive neurodegeneration and death [12].
78 H3K27me3 may be required in terminally differentiated neurons to persistently repress genes
79 that have the potential to drive trans-differentiation to alternate cell fates. For example, in a
80 longitudinal study of postmitotic dopamine neurons undergoing directed differentiation in
81 culture, poised RNA Pol-II was found to colocalize with H3K27me3 at promoters of genes
82 encoding non-neuronal transcription factors (TFs) [13]. A separate study showed knockout of
83 the PRC2 component EED resulted in transcriptional de-repression of a set of TFs that have the
84 capacity to drive cellular reprogramming [12]. A non-exclusive possibility is that H3K27me3 is
85 required to maintain the expression of genes that define the terminal neuronal fate. Consistent
86 with this model, deleting EED in developing postmitotic dopamine or serotonin neurons *in vivo*
87 leads not only to loss of H3K27me3 but also to reduced expression of tyrosine hydroxylase (TH)
88 and tryptophan hydroxylase 2 (TPH2), respectively, which, as the key enzymes that mediate
89 dopamine and serotonin synthesis, define the transmitter phenotype of these
90 neuromodulatory neurons [14].
91
92 These data suggest that dynamic changes in H3K27me3 in postmitotic neurons could
93 play a role in plasticity of cell fate or function and raise the question of the molecular
94 mechanisms that can control this distribution. The global depletion of H3K27me3 in neurons
95 takes months to appear after deletion of EZH1/2 [12] revealing that this histone modification is
96 remarkably stable across the bulk of the genome. Furthermore, whereas histone replacement is
97 a major mechanism of H3K27me3 removal in dividing cells [15], histone turnover is very slow in
98 postmitotic neurons [16]. Instead, lysine demethylases may have a privileged role in the local
99 regulation of histone methylation patterns in postmitotic neurons [17]. Both *Kdm6a* and *Kdm6b*
100 are expressed in neurons over the course of brain development, though only *Kdm6b* shows
101 enhanced expression following exposure of cells to neuronal differentiation cues [11, 18-20].
102 Germline knockout of *Kdm6b* does not impair the gross architecture of the embryonic brain,
103 but it does result in perinatal lethality caused by disruption of respiratory circuit maturation
104 [20]. To identify functions of histone H3K27 demethylation in postmitotic stages of

105 neurodevelopment, we previously conditionally deleted *Kdm6a* and *Kdm6b* in *Atoh1*-expressing
106 cerebellar granule neuron (CGN) progenitors of the mouse. We used CGNs to model
107 neurodevelopment because they comprise more than 99% of all neurons [21] and 85% of cells
108 [22] in the cerebellum, enabling the *in vivo* comparison of chromatin across CGN
109 developmental states with limited contamination from other cell types. When purified and
110 placed in *ex vivo* culture, CGN progenitors coordinately exit the cell cycle, minimizing
111 heterogeneity of cell developmental stage across the population [23]. In both preparations,
112 gene transcription programs change over time coincident with changes in CGN biology (*e.g.,*
113 proliferation, migration, synapse formation, synapse maturation [24, 25]). Loss of *Kdm6a/b* had
114 no effect on postnatal morphogenesis of the cerebellum, demonstrating these enzymes are not
115 required *in vivo* for regulation of CGN progenitor proliferation. However knockdown of *Kdm6b*
116 in cultured CGNs impaired the developmental induction of genes during the period of
117 postmitotic neuronal maturation [11]. Based on these data, we hypothesized that H3K27me3
118 may serve as a temporal gatekeeper of these maturation genes, delaying their activation
119 beyond the immediate period of terminal differentiation to the neuronal fate.
120
121 Here we investigated the contribution of H3K27me3 dynamics to changing programs of
122 gene transcription in maturing CGNs. We used ChIP-seq and CUT&RUN to identify the genomic
123 location and timing of differential sites of H3K27me3 enrichment across the genome of CGNs
124 developing *in vivo* and in culture. We observed that H3K27me3 distributions continue to
125 change even after fate committed CGN progenitors exit the cell cycle, and that the loss of
126 H3K27me3 at gene promoters is associated with the activation of genes induced as neurons
127 mature. We used both genetic and pharmacological approaches to disrupt the action of
128 H3K27me3 regulatory enzymes and show evidence of roles for both the lysine demethylase
129 KDM6B and the lysine methyltransferase EZH2 in the induction of a postmitotic program of
130 gene transcription that underlies functional maturation of CGNs. Taken together, our data
131 advance understanding of how programs of gene expression are temporally orchestrated in
132 maturing neurons.
133

134 # Materials and Methods

135

136 **Animal Husbandry**

137 We performed all procedures under an approved protocol from the Duke University Institutional
138 Animal Care and Use Committee. *Kdm6b* floxed mice described in [26] were obtained from
139 Jackson Labs (Stock #029615, RRID #IMSR_JAX:029615). These mice contain *loxP* sites flanking
140 exon 14-20, encoding the catalytic Jumonji-C domain, of the mouse *Kdm6b* gene on chromosome
141 11. *Atoh1-cre* mice were obtained from Jackson Labs (Stock #011104, RRID #IMSR_JAX:011104).
142 Mice were genotyped by ear clipping at the time of weaning using protocols described on the
143 Jackson Labs website. CD-1 IGS mice (#Strain 022, #IMSR_CRL:022) and C57BL/6NCrl mice
144 (#Strain 027, RRID #IMSR_CRL:027) were obtained from Charles River Laboratories. Both male
145 and female mice were used for all experiments in this study.

146

147 **CGN Culture**

148 Cerebella of CD1-IGS mice were dissected at P6-P8. Cells were dissociated and run on a Percoll
149 gradient to isolate cerebellar granule neuron progenitors (GNPs) as previously described [27].
150 GNPs were plated at a density of 1 million cells/well in a 24-well plate for RNA or protein isolation.
151 At day *in vitro* 2 (DIV2) CGNs were treated with 1 µM Cytosine Arabinoside (AraC) (Sigma #C1768)
152 to block division of any non-neuronal cells. KDM6 and EZH2 inhibitors were added at the doses
153 and days described in the text.

154

155 **RT-qPCR**

156 CGNs were lysed in TRIzol Reagent (Thermo #15596026) at a volume of 0.25 mL per 1 million cells
157 for RNA purification. Isolated RNA was analyzed using a nanodrop to determine concentration
158 and purity, after which it was treated with DNase I (NEB #M0303S). We made Oligo(dT) primed
159 cDNA using SuperscriptII Reverse Transcriptase (Invitrogen #19064014). qPCR was carried out on
160 an Applied Biosystems Quantstudio 3 Thermal cycler using Power SYBR Green PCR Master Mix
161 (Thermo #4367659) and PCR primers targeting the gene/locus of interest (**Supplementary**
162 **Information, Table S1)**.

163 **RNA-seq**

164 RNA for RNA-seq was obtained by processing cerebellar tissue or CGN cultures with Trizol reagent
165 followed by clean up on the Zymo Direct-zol RNA miniprep kit (Zymo #R2052). RNA purity was
166 measured to ensure samples had A260/280 and A260/230 values > 1.9. RNA was then polyA
167 enriched and 150 bp paired-end sequencing was performed by Novogene, Inc on an Illumina Hi-
168 seq 2000 machine.

169

170 **Chromatin Immunoprecipitation**

171 **Cerebellar Tissue:** We pooled cerebellum from three C57BL/6NCrl (Charles River Laboratories
172 IMSR Cat# CRL:027, RRID: IMSR_CRL:027) P7 mice, two P14 mice and one P60 mouse for each
173 biological replicate. Both male and female mice were used. Cerebellum samples were dounced
174 in a glass homogenizer containing 2 ml of 1% formaldehyde (w/v) PBS buffer per sample and
175 kept at 25 °C for 15 min, washed twice with cold PBS, lysed in 600 µl lysis buffer (1% SDS (w/v),
176 10 mM EDTA, and 50 mM Tris, pH 8.1). The cross-linked material was sonicated with a
177 Bioruptor (Diagenode), with output set to "high" with 30 s on/off cycles to an average size
178 range of 150–350 bp which was then determined by agarose gel electrophoresis. Sonicated
179 chromatin was centrifuged for 10 minutes at 14000 RPM at 4°C, after which the supernatant
180 was diluted 10-fold in dilution buffer (0.01% SDS, 1.1% Triton X-100, 1.2 mM EDTA, 16.7 mM
181 Tris-HCl, pH 8.1, 167 mM NaCl). Prior to immunoprecipitation, 6 µl of antibody (anti-H3K27Me3,
182 Active Motif 39155, RRID: AB_2561020) was incubated with 100 µl of Dynabeads Protein G
183 (Invitrogen 10004D) in PBS for 4-6h at 4 °C. The antibody-bead conjugate was then washed
184 twice with cold PBS, and added to 6 ml of cell lysis for overnight immunoprecipitation at 4˚C.
185 The following day, bead-bound DNA-protein complexes were washed, eluted, and purified
186 using a PCR purification kit (Cat# 28104, Qiagen). ChIP-seq libraries were made using the
187 MicroPlex Library Preparation kit V2 (C05010012, Diagenode); and 50 bp single-end sequencing
188 was performed at the Duke Sequencing and Analysis Core Resource on a Hi-Seq 2000 machine.
189 Three independent biological replicates were performed for each antibody and developmental
190 time point and ChIP reagents were prepared according to the Millipore 17–295 ChIP kit.

191

192 **Nuclear Isolation of CGNs for CUT&RUN**

193 CGNs were scraped into 1X DPBS at 0.25 mL per 1 million cells and then 'pop-spun' according to
194 the REAP method [28], until the rotor reached 7000 rpm. Pellets were then washed once with 1X
195 DPBS and pop-spun again, after which they were resuspended in Nuclei Isolation Buffer (20 mM
196 HEPES pH 7.9, 10 mM KCl, 2 mM Spermidine, 0.1% v/v Triton X-100, 20% v/v glycerol), incubated
197 on ice for 5 minutes and then spun at 2,000g for 5 min at 4˚C. After this step the supernatant was
198 removed, and pelleted nuclei were then resuspended in Nuclei Storage Buffer (20 mM Tris-HCl
199 pH 8.0, 75 mM NaCl, 0.5 mM EDTA, 50% v/v glycerol, 1 mM DTT, 0.1 mM PMSF) and stored in -
200 80˚C until ready to process.

201

202 **CUT&RUN**

203 CUT&RUN was performed on nuclei isolated from CGN cultures using the CUTANA
204 ChIC/CUT&RUN kit (EpiCypher #14-1408) as per manufacturer guidelines. Specific changes made
205 to the protocol are noted here. Nuclei in Nuclei Storage Buffer were pelleted and resuspended in
206 Nuclei Isolation Buffer. Nuclei were then incubated with activated ConA beads. Antibodies used
207 for CUT&RUN were: H3K27me3 (Active Motif 39155, RRID: AB_2561020), H3K4me3 and IgG
208 (positive and negative controls included in kit). CUT&RUN libraries were made using the NEB
209 Ultra II DNA Library Prep Kit for Illumina (NEB #E7645L), and NEBNext Multiplex Oligos for
210 Illumina (96 Unique Dual Index Primer Pairs) (NEB #E6440S). Library cleanup was performed prior
211 to and after PCR amplification using 0.8X Kapa Hyperpure beads (Roche #08963851001). PCR
212 amplification was performed with the following parameters as described in the EpiCypher
213 CUT&RUN kit: 1) 98˚C, 45 sec; 2) 98˚C, 15 sec; 60˚C, 10 sec x 14 cycles; 3) 72˚C, 60 sec. Libraries
214 were then pooled and 50 bp paired-end sequencing was performed at the Duke Sequencing and
215 Analysis Core Resource on a NovaSeq 6000 S-Prime flow cell.

216

217 **Sequencing Data Analysis**

218 **ChIP-seq:**

219 ChIP-seq reads were quality scored and screened through fastQC, trimmed for adapter
220 sequences using Trimmomatic 0.38 and then aligned to the mouse GRCm38.p4 reference

221 genome using STAR 2.7.2b. Alignments were filtered for mapped reads using samtools and then
222 normalized using the bamCoverage function of the deepTools2.0 suite. ChIP-seq tracks were
223 generated using bamCoverage, to generate continuous BigWig files. Peak calling was performed
224 using Macs2, with parameters for broad peaks and an FDR threshold of 0.01. The R package
225 DESeq2 [29] was used for read-count normalization and differential binding analysis. R package
226 ChIPseeker [30] was used to annotate ChIP-seq peaks using a window of TSS $\pm$ 3000.
227 'Promoters' is a group of ChIPseeker terms 'Promoter (<=1kb), Promoter (1-2 kb) and Promoter
228 (2-3 kb). Gene Body is a group of terms 5' UTR, 3' UTR, Intron and Exon.
229
230 **CUT&RUN:**
231 CUT&RUN reads were processed the same as ChIP-seq reads until peak-calling. Peak calling was
232 performed using Macs2, with parameters for broad peaks and an FDR threshold of 0.1.
233 Metagene plots were created using SeqPlots [31], by inputting bigwig and BED files and setting
234 a window of TSS +/- 1000 bp.
235
236 **RNA-seq**
237 RNA-seq reads were processed similarly to ChIP-seq reads until and excluding peak calling. Read
238 counts for genes were generated using HTseq2 count, with feature type set to 'exon', and the
239 Gencode GRCm38.p4 GTF annotation file. DESeq2 was used for read-count normalization and
240 differential expression analysis.
241
242 **Data Processing**
243 Heatmaps were generated using the Broad Institute's Morpheus tool:
244 https://software.broadinstitute.org/Morpheus, with the following clustering parameters:
245 hierarchical clustering, complete linkage, one minus spearman rank correlation, cluster by rows.
246 VST-transformed counts used to generate heatmaps and clusters are provided in Table S2. Gene
247 ontology analysis was performed using the GO consortium GO tool [32, 33] using terms related
248 to 'biological process'.
249

250 **Western Blot**

251 **Cerebellar Tissue:** For preparation of protein lysates from cerebellar tissue, we pooled
252 cerebellum from two P7 mice, one P14 and one P60 mouse for each biological replicate.
253 Cerebellum samples were dounced 50 times with PBS in glass homogenizer, centrifuged at 8000
254 x g for 5 minutes, and washed twice by cold PBS, then pellets were re-suspended in 300 µL
255 extraction buffer (10 mM HEPES, pH 7.9, 1.5 mM $MgCl_2$, 10 mM KCl), supplemented with 1X
256 protease inhibitor cocktail (Roche, Indianapolis, IN). Thereafter, 60µL of 1N HCl was added to
257 the cell lysates and kept on ice for 30 minutes, following which the cell lysates were centrifuged
258 at 11,000 x g for 10 minutes at 4 ºC. Protein concentration of acid-soluble supernatants was
259 measured using Pierce BCA protein assay kit (Cat # 23227, Thermo). 20 µg of acid-soluble
260 supernatant was used for western blots. Samples were loaded onto wells of a 10-20% gradient
261 gel and run at 150V for 30-40 min in running buffer (25 mM Tris-HCl, 192 mM Glycine, 0.1% w/v
262 SDS) after which protein was transferred onto a PVDF membrane (BioRad #1620177) in transfer
263 buffer (25 mM Tris-HCl, 192 mM Glycine, 20% v/v Methanol) for 1 hour at 100V or overnight at
264 30V. The membrane was blocked for 1 hour in 5% (w/v) BSA (Sigma #A3059) in TBST. After the
265 blocking step, the membrane was incubated with primary antibody overnight at 4˚C. The
266 following day, primary antibody was removed, after which the membranes were washed three
267 times with TBST for 5 minutes each, incubated with secondary antibody for 1 hour, and then
268 again washed three times with TBST for 5 minutes each. At the end of this, membranes were
269 imaged using the Li-Cor Odyssey using appropriate exposure times for the target antibodies.
270

271 **CGN Culture**: Cells were scraped into PBS from 6 well plates at the relevant endpoints,
272 centrifuged at 200 x g for 5 minutes, and washed twice with PBS. Pellets were then
273 resuspended in 100 µL of extraction buffer (described above), after which 20 µL of 1N HCl was
274 added. Samples were hereafter processed as described above.
275

276 **Antibodies:** The antibodies used were H3K27Ac (Abcam ab4729), H3K27Me3 (Active Motif
277 39155, RRID: AB_2561020), and Total H3 (Tissue: Millipore 05-499, Culture: Cell Signaling 9715).
278 Western blot signals were detected by Li-Cor Odyssey InfraRed Imaging System (Lincoln, NE)

279 with the secondary antibodies, CF770 goat anti-Rabbit, (Biotium 20078) and CF 680 goat anti-
280 mouse, (Biotium 20065). Protein bands were quantified using ImageJ.
281
282 **GEO Accession Codes**
283 H3K27me3 ChIP-seq data for P7, P14 and P60 cerebellum, WT and *Kdm6b*-cKO cerebellum;
284 RNA-seq data for WT and *Kdm6b*-cKO cerebellum; CUT&RUN data for CGNs can be accessed at
285 GEO: GSE212441. RNA-seq data for P7, P14 and P60 cerebellum and DIV0 and DIV7 CGNs,
286 H3K27ac, ZIC1/2 ChIP-seq data and DHS-seq data for P7 and P60 cerebellum were adapted
287 from Frank et. al 2015 [25].
288
289 **Author Contributions**
290 Conceptualization: V.R., F.L. and A.E.W.; Methodology: V.R., F.L., U.C., and A.E.W.; Formal
291 Analysis: V.R., M.M.; Investigation V.R.; Resources, A.E.W.; Writing: V.R., A.E.W.; Funding
292 Acquisition: A.E.W.
293
294 **Acknowledgements**
295 Fig schematics in Fig 1A, 3A and 5A were created using biorender.com.

296 # Results

297
298 Cerebellar Maturation Involves Dynamic, Genome-Wide Changes in H3K27me3 Distribution
299 To measure H3K27me3 dynamics during cerebellar maturation, we harvested cerebellar
300 cortex from C57BL/6NCrl mice at postnatal days 7, 14, and 60 (Fig. 1A). At P7, about half of all
301 cells in the mouse cerebellum are proliferating granule neuron precursors (GNPs) whereas the
302 rest are immature, postmitotic cerebellar granule neurons (CGNs). By P14 GNP cell division has
303 ceased, and the cerebellum is composed of immature postmitotic CGNs that are migrating to the
304 inner granule layer (IGL) where they receive synapses and fully mature by P60 [22, 25]. Western
305 blot of acid extracted histones showed a significant global increase in total H3K27me3 levels from
306 P7 to P14 that was maintained at P60 (Fig 1B), whereas total H3K27ac fell in a similar temporal

307 pattern (Fig. S1A). These data are consistent with the PRC2-dependent restriction of cell potential
308 upon terminal differentiation [4].
309
310 However, when we assessed the genomic location of H3K27me3 by ChIP-seq (Fig S1B) we
311 observed local losses as well as gain in H3K27me3 enrichment between developmental stages
312 (Fig 1C). This was true even when comparing P14 with P60 (Fig 1C), demonstrating that changes
313 in H3K27me3 distributions occur during postmitotic stages of neuronal maturation, well after the
314 period of terminal cell fate commitment has ended (Fig S1C). We stratified differential H3K27me3
315 ChIP-seq peaks by their genomic location with respect to proximal gene promoters, gene bodies
316 or intergenic regions (Fig 1D), and found a consistent overrepresentation of proximal gene
317 promoters among developmentally demethylated peaks for all three comparisons. By contrast,
318 H3K27me3 ChIP-seq peaks differentially gained between all three comparisons did not differ
319 from the global distribution of H3K27me3, which was distributed across gene-body and distal
320 intergenic regions as well as proximal promoters. The percentage of total H3K27me3-positive
321 promoters gradually decreased by ~2-fold from P7 to P60, while that of H3K27me3-positive distal
322 intergenic regions increased, and that of gene bodies stayed about the same over time (Fig 1E).
323 Additionally, the total number of H3K27me3 peaks called centered within a 3 kb window around
324 the TSS appeared to gradually decrease from P7 to P60 (Fig 1E). These data demonstrate that in
325 CGNs H3K27me3 patterns are locally regulated in postmitotic neurons, suggesting a function for
326 PRC2-dependent gene regulation in neurons that extends beyond the restriction of cell fate
327 commitment.
328
329 <u>H3K27me3 Dynamics at Promoters During Cerebellar Maturation Inversely Correlate with Gene</u>
330 <u>Expression</u>
331 We filtered differential H3K27me3-peaks for those occurring at promoters because these
332 regions can be directly mapped to their likely target gene for transcriptional regulation. We then
333 asked whether peaks that were up- and downregulated over stages of CGN differentiation were
334 found at genes that can be stratified according to cellular function. Examples of genes with
335 promoter-associated peaks lost or gained from P7 to P60, respectively, were the genes encoding

336 the mature NMDA-type glutamate receptor *Grin2c* which is strongly expressed in mature CGNs
337 [11] and the cell-proliferation factor *Mycn,* which is expressed only in GNPs [34] (Fig 1F). This is
338 consistent with the hypothesis that changes in the levels of promoter H3K27me3 inversely
339 correlate with changes in gene expression over development.
340
341 To determine if the correlation of H3K27me3 demethylation with transcriptional
342 maturation held more broadly, we first performed hierarchical clustering on all differential
343 H3K27me3 ChIP-seq peaks and identified 3 major clusters with differing direction and timing of
344 change (Fig 2A). The first cluster, which we termed 'H3K27me3 Up,' contained peaks that gained
345 methylation as early as P14 and maintained methylation during CGN maturation. Gene Ontology
346 (GO) analysis demonstrated that these peaks were enriched for genes associated with progenitor
347 functional terms related to cell proliferation and morphogenesis. The next two clusters included
348 demethylated peaks, that we termed 'H3K27me3 Down (Fast)' and 'H3K27me3 Down (Slow)'
349 respectively, depending on whether they changed between P7 and P14 or between P14 and P60.
350 Both clusters were enriched for neuronal GO terms. Because developmentally gained peaks
351 showed a broader distribution than just promoters, we also performed the same type of filtering
352 and hierarchical clustering for differential H3K27me3 peaks overlying gene bodies (Fig S2) and
353 found two clusters with significantly enriched GO terms. This resulted in three clusters, two of
354 which contained peaks that gained and lost methylation respectively at gene-bodies. Both these
355 clusters were enriched for neuronal GO terms including early CGN-maturation genes. Together,
356 these data show that H3K27me3 dynamics are distinct across distinct genomic locations.
357
358 We then asked if H3K27me3 dynamics at gene promoters were associated with the
359 expression of the corresponding RNA transcript across CGN maturation (Fig 2B, C). For this
360 purpose, we compared our H3K27me3 ChIP-seq to a dataset of gene expression at the same time
361 points from our previous study [25]. We found that 'H3K27me3 Up' peaks at gene promoters
362 were significantly associated with a decrease in expression of the associated gene over the same
363 period of developmental time and 'H3K27me3 Down' peaks were associated with an increase in
364 gene expression. Among the H3K27me3 Down peaks, 'Fast' peaks were associated with a

365 significantly greater magnitude of gene induction than 'Slow' peaks between P7 and P14, but
366 'Slow' peaks were associated with a significantly greater magnitude of gene induction than 'Fast'
367 peaks between P14 and P60. There was no significant difference between 'Fast' and 'Slow' peaks
368 from P7 to P60 indicating that it is the timing not the magnitude of differential developmental
369 gene expression that defines the two clusters. These data show that the kinetics of H3K27me3
370 demethylation at gene promoters are associated with the timing of gene expression changes in
371 postmitotic neurons, which allows for multiple postmitotic waves of gene expression (Fig. 2C).
372
373 <u>*Kdm6b*-cKO Impairs CGN Maturation via Promoter Hypermethylation</u>
374 The developmental loss of H3K27me3 at a subset of gene promoters in CGNs could occur
375 through changes in expression of the enzymes that maintain or remove these histone
376 modifications. At the level of gene expression, RNA-seq counts of the H3K27 methyltransferases
377 *Ezh1/2* and the H3K27 demethylases *Kdm6a*/b showed that although there was a developmental
378 switch between the dominant reader and writer enzymes, the overall expression levels of each
379 class of enzyme did not change over time (Fig S1D). However, previous *in situs* from our lab
380 demonstrated that *Kdm6b* expression is transiently induced in newborn CGNs in the inner EGL,
381 and we further showed that shRNA-mediated knockdown of *Kdm6b* in cultured CGNs impairs the
382 expression of a subset of developmentally induced genes [11]. Thus, we considered the
383 possibility that KDM6B might mediate postmitotic loss of H3K27me3 at a subset of
384 developmentally induced gene promoters in the developing cerebellum *in vivo* to promote their
385 transcriptional induction. To test this hypothesis, we conditionally knocked out *Kdm6b* in
386 cerebellar granule neuron precursor cells (GNPs) *in vivo* by crossing heterozygous transgenic
387 *Atoh1-Cre* mice with *Kdm6b*$^{fl/fl}$ mice. We then harvested cerebellar tissue from littermates that
388 were either *Kdm6b*$^{fl/fl}$ (WT) or *Atoh1-Cre; Kdm6b*$^{fl/fl}$ (*Kdm6b*-cKO) at P14 as an intermediate
389 developmental time point for CGN maturation [25] (Fig 3A). We processed this tissue to perform
390 either RNA-seq (Fig S3A) or ChIP-seq for H3K27me3 (Fig S3B). We used DESeq2 to compute
391 differentially enriched H3K27me3 ChIP peaks between WT and *Kdm6b*-cKO tissue at P14, and
392 obtained 250 upregulated peaks, and 327 downregulated peaks (FDR < 0.05, |Log2FC| > 1) (Fig
393 3B). We then mapped these differential peaks to their genomic location (Fig 3C). We found peaks

394 with elevated levels of H3K27me3 in *Kdm6b*-cKO mice to be significantly more likely to be within
395 gene promoters compared with the overall distribution of peaks or the distribution of peaks that
396 had reduced H3K27me3 in *Kdm6b*-cKO mice. We observed that the percentage of promoter
397 associated H3K27me3 peaks decreased between WT and *Kdm6b*-cKO mice, while peaks in distal
398 intergenic regions and gene-bodies increased (Fig S3C). The total number of H3K27me3 peaks
399 called within a 3 kb window around the TSS appeared to increase due to *Kdm6b*-cKO (Fig S3C).
400 The genes containing promoters with increased H3K27me3 in the *Kdm6b*-cKO were enriched for
401 neuronal GO terms (Fig 3D), whereas those containing promoters with decreased H3K27me3 in
402 the *Kdm6b*-cKO mice failed to pull any significant GO terms. Overall, these observations mirror
403 our findings of H3K27 demethylation at the promoters of neuronal maturation genes and
404 suggests that KDM6B may mediate that process.
405
406 To determine the relationship between H3K27me3 levels at promoters and gene
407 expression in the *Kdm6b*-cKO mice, we computed the correlation between *Kdm6b*-cKO
408 associated differential H3K27me3 enrichment at promoter regions, with the expression of the
409 associated gene in WT and *Kdm6b*-cKO mice. These data showed that the gain of H3K27me3 is
410 associated with a significant loss of gene expression (Fig. 3E) as exemplified by the synaptic genes
411 *Grm4* and *Gabbr2* (Fig 3F). By contrast, promoters that lost H3K27me3 in *Kdm6b*-cKO mice
412 showed no significant difference in gene expression (Fig.3E). These data suggest that
413 developmental loss of H3K27me3 at the promoters of genes induced in CGNs during postmitotic
414 maturation is facilitated by KDM6B, and that this loss promotes the developmental induction of
415 gene expression.
416
417 <u>H3K27me3 Removal at CGN-Maturation Gene Promoters is Associated with H3K27ac Enrichment</u>
418 <u>and Increased Chromatin Accessibility</u>
419 Previously we showed CGN maturation to occur in concert with broad, genome-wide
420 changes in H3K27ac [25]. Indeed, 26866 peaks were gained, and 28227 peaks were lost from P7
421 to P60 (Fig S4A). To ask whether H3K27me3 removal at promoters overlapped with the gain of
422 H3K27ac, we computed the overlap between genes containing promoter peaks that were

423 H3K27ac Up (|L2FC| > 0, FDR < 0.05) and H3K27me3 Down (Fig S4B). We observed that only a
424 subset of genes that gained H3K27ac also lost H3K27me3 at P60. H3K27ac Up genes that were
425 H3K27me3 Down (912 genes), or not H3K27me3 Down (4208 genes) were both highly enriched
426 for neuronal GO terms (Fig S4C). To determine what characterizes the subset of promoters that
427 become demethylated we sought to ask what transcription factors might be found at these gene
428 promoters compared to all H3K27me3-positive promoters. To conduct an unbiased screen, we
429 first utilized the tool called Binding Analysis for Regulation of Transcription (BART) [35], which
430 calculates enrichments of previously published ChIP-seq TF binding profiles within a defined set
431 of genomic regions. We first filtered our ChIP-seq data for genes associated with the 'H3K27me3-
432 Down' peak cluster described in Fig 2A, combining 'Down (Fast)', and 'Down (Slow)' clusters, and
433 obtained predicted transcription factors (TF) whose binding significantly overlaps these gene
434 promoters. We compared the enrichment statistics of TFs enriched in these clusters to those
435 derived from all H3K27me3– promoter associated genes (Fig 4A). As expected, we found PRC2
436 components EZH2, JARID2, SUZ12 to be significantly enriched across both the H3K27me3-Down
437 cluster and all H3K27me3-promoter associated genes. However, we found only the H3K27me3-
438 Down cluster to be significantly enriched for the putative binding of transcription factors ZIC1
439 and ZIC2, which previous work from our group has shown to be a driver of CGN maturation [25].
440 Importantly, when we assessed the 'H3K27me3-Down (Fast)', and 'H3K27me3-Down (Slow)'
441 clusters separately (Fig S5A), they were also enriched for the binding of ZIC1 and ZIC2, which is
442 consistent with evidence [25] that these TFs function at multiple stages of CGN differentiation.
443 By contrast, when we performed the same analysis for the 'H3K27me3-Up' cluster (Fig S5A), we
444 found this set of promoters was significantly enriched for the binding of a distinct set of TFs
445 involved in cell differentiation, namely SOX3, FOXF1, SHOX2, POU3F2 as well as histone
446 deacetylation (HDAC1) [36].
447
448 To directly compare changes in ZIC1/2 TF binding to changes in H3K27me3 across CGN
449 development, we re-analyzed our previously published ZIC1/2 ChIP-seq data [25] and identified
450 gene promoters with increased ZIC binding at P60 compared with P7. We termed these genes
451 'ZIC Up' and first compared them to the H3K27me3-Down cluster. We found that 56% of

452 H3K27me3-Down genes were also ZIC-Up, and that these genes were enriched for neuronal GO
453 terms. As a control, we compared 'ZIC Up' genes to H3K27me3-Up genes (Fig. S5B) and only found
454 an overlap of only 11%. We repeated this analysis with the H3K27me3 ChIP-seq peaks that were
455 differential at P14 between WT and *Kdm6b*-cKO (Fig. 3) and found a similar enrichment of
456 putative ZIC1 and ZIC2 binding within gene promoters associated with H3K27me3 peaks 'Up in
457 *Kdm6b*-cKO' (Fig 4B), but not 'Down in *Kdm6b*-cKO' (Fig S5B). 72% of the 'H3K27me3 Up in
458 *Kdm6b*-cKO' genes were also 'ZIC Up', whereas only 9% of demethylated genes were also 'ZIC
459 Up'. As examples of gene promoters that belong to both the H3K27me3-Down cluster, and
460 H3K27me3 Up peaks due to *Kdm6b*-cKO, we show tracks for *Grin2c*, *Grm4* and *Kcna1* that are
461 strongly enriched for ZIC1/2 at their promoters at P60 (Fig S5C).
462
463 We have shown previously [11] that increased ZIC1/2 binding strongly correlates with the
464 developmental enrichment of H3K27ac and increased chromatin accessibility during cerebellar
465 maturation. Given the strong enrichment of ZIC1/2 binding within the H3K27me3-Down cluster
466 during development, and H3K27me3 Up peaks due to *Kdm6b*-cKO, we wanted to ask whether
467 H3K27me3 turnover during cerebellar maturation is associated with H3K27ac enrichment and
468 changes in chromatin accessibility. As such we computed the distribution of Log2FC values from
469 our previously published H3K27ac-ChIP-seq and DNAse Hypersensitivity data [25] comparing P7
470 and P60 cerebellum and filtered these distributions for those related to peaks belonging to our
471 differential H3K27me3 promoter clusters. Indeed, H3K27me3 Down peaks at P60 were
472 significantly associated with an increase in H3K27ac enrichment and DNAse hypersensitivity (Fig
473 4C, left). H3K27me3-Up peaks due to *Kdm6b*-cKO conversely were associated with genes that
474 became enriched with H3K27ac, and DNAse hypersensitive regions at P60 (Fig 4C, right).
475 Visualizing tracks for both H3K27ac ChIP-seq and DNAse hypersensitivity data at CGN maturation
476 genes *Grin2c* and *Grm4*, which we previously showed lost H3K27me3 during development and
477 gained H3K27me3 due to *Kdm6b*-cKO, both gain H3K27ac and chromatin accessibility at their
478 promoters (Fig 4D). Thus, these data provide further evidence that the postmitotic removal of
479 H3K27me3 from a subset of gene promoters is important for the coordinated induction of gene
480 expression that underlies neuronal maturation.

481

482 Modulation of H3K27me3 Turnover Mediates CGN Maturation Gene-Regulation in Culture

483 To determine the functional consequences of modulating H3K27me3 at CGN-maturation
484 gene promoters or gene bodies we used cultures of primary mouse CGNs as context for
485 pharmacological manipulation of histone regulatory enzymes. When GNPs isolated from P6-8
486 mouse cerebellum are placed in culture they show changes in gene expression over the course
487 of 7 days [25] (Fig. S6B). We performed CUT&RUN-seq to measure genome-wide changes in
488 H3K27me3 after 1, 3, 5 and 7 days *in vitro* (DIV) (Fig 5B, S6A). We found methylation to be gained
489 quickly after cell cycle exit, with 1688 peaks significantly up between DIV1 and DIV3 CGNs,
490 followed by 109 peaks between DIV3 and DIV5, and 2 peaks between DIV5 and DIV7 CGNs (Fig
491 S6B). Like our observations *in vivo* (Fig. 1, 2), we saw that demethylation occurred more gradually,
492 with 477 peaks significantly down between DIV1 and DIV3 CGNs, followed by 227 and 25 peaks
493 between DIV3 and DIV5, and DIV5 and DIV7 CGNs respectively. Again, consistent with our
494 findings *in vivo*, we found demethylation to occur primarily at promoters (Fig 5C, Fig S6C, D), and
495 methylation to occur more uniformly, including at gene-bodies and distal intergenic regions.
496 When we filtered for differential H3K27me3 peaks at gene promoters, they clustered in two
497 groups that were methylated or demethylated at DIV7 (Fig 5D). Genes whose promoters were in
498 the 'Methylated at DIV7' cluster were associated with cell fate specification GO terms as
499 predicted by canonical PRC functions. Conversely, genes whose promoters were in the
500 'Demethylated at DIV7' cluster were associated with functional neuronal GO terms. We observed
501 mature synaptic genes such as *Grin2c* and *Grm4* to lose H3K27me3 (Fig 5E upper), and
502 proliferation genes expressed in GNPs such as *Myc* and *Atoh1* to gain H3K27me3 in culture (Fig
503 5E lower). Finally, we stratified our previously published RNA-seq data between DIV0 and DIV7
504 CGNs by their respective methylation status ('Methylated at DIV7' or 'Demethylated at DIV7'
505 cluster) and calculated the distribution of Log2FC (Fig 5F). We found peaks associated with the
506 'Methylated at DIV7' cluster to have a significant reduction in gene expression, and those
507 associated with the 'Demethylated at DIV7' cluster to have a significant gain in gene expression
508 by DIV7 (Fig 5F). These data show that we can use this CGN culture system to explore mechanisms

509 and causality with respect to the enzymes mediating H3K27me3 turnover and gene regulation
510 during CGN maturation.
511
512 To determine the functional contribution of H3K27me3 regulation to CGN-maturation
513 gene expression, we treated CGN cultures at DIV1 with small molecule inhibitors of either EZH2
514 or KDM6A/B, called GSK-126 and GSK-J4 respectively, and measured the consequences for cell
515 viability, histone modification, and gene expression at DIV5. Because these drugs have not been
516 widely used in primary neurons, we first performed a cell viability assay and measured the IC_{50}
517 values of both drugs. We determine the IC_{50} values to be ~3.07 µM for GSK-J4 and ~7.32 µM for
518 GSK-126, respectively (Fig S7A). For the KDM6B inhibitor, the IC_{50} was nearly 10-fold below the
519 dose (25 µM) used in the original characterization studies to block the histone demethylase
520 activity of these enzymes [37]. Thus, we sought to determine if these drug could block enzymatic
521 function in viable cells. Choosing concentrations below the measured IC_{50} values, we first
522 measured global levels of H3K27me3 by western blot (Fig 6A), after treating with 0, 0.5, 1.0 and
523 2.0 µM of either drug. Treatment of CGNs with GSK-126 caused a dose-dependent loss of
524 H3K27me3 validating the method. By contrast, GSK-J4 treatment failed to cause any dose-
525 dependent change in H3K27me3 detected by western. GSK-J4 treatment also failed to modulate
526 levels of H3K27ac while GSK-126 treatment appeared to cause a global increase (Fig S7B). This
527 finding is consistent with the idea that H3K27me3 and H3K27ac are mutually exclusive
528 modifications that oppose each other's functions [38].
529
530 Given our evidence that KDM6B facilitates demethylation of a subset of gene promoters
531 over development (Fig 2) in the absence of global reductions in H3K27me3 (Fig 1), we asked if
532 there might be local changes in H3K27me3 after GSK-J4 treatment. We treated CGNs daily with
533 1 µM of GSK-J4 between DIV1-DIV5 and then assessed H3K27me3 peaks across the genome by
534 CUT&RUN-seq to determine if there were local increases in H3K27me3 at a subset of genes (Fig
535 S7C-D). We failed to observe any significant changes in H3K27me3 enrichment across the
536 genome at this concentration of GSK-J4 (Fig S7E), with biological replicate being the primary
537 factor for variation in this dataset (Fig S7D). We did observe a small increase in the total number

538 of H3K27me3 peaks called between DMSO and 1µM GSK-J4 treated cells, though the distribution
539 of peaks between different genomic regions stayed constant (Fig S7C), and we found 1µM GSK-
540 J4 treatment to slightly decrease mRNA levels of specific neuronal function genes (Fig S7F).
541 Nonetheless, we conclude that the therapeutic range of GSK-J4 is too small in our CGNs cultures
542 to permit useful interpretations of the inhibition of KDM6-dependent demethylation for this
543 study.
544
545 Our data showed that EZH2-inhibiting doses of GSK-126 were compatible with CGN
546 viability, thus we then used CUT&RUN-seq for H3K27me3 on CGNs GSK-126 (Fig 6, Fig S8A). Most
547 of the regions that showed differential methylation following GSK-126 treatment had lower
548 levels of H3K27me3 in GSK-126 treated neurons, consistent with the inhibition of this histone
549 methyltransferase (Fig 6B). A much smaller number of peaks showed increases in H3K27me3,
550 which may arise from secondary effects of EZH2 inhibition on other processes that impact
551 H3K27me3 distributions such as EZH1 function [39] or histone turnover [40]. Regions that lost
552 H3K27me3 after GSK-126 treatment showed a similar genomic distribution to the overall
553 distribution of H3K27me3 peaks in CGNs (Fig S8B-C). Demethylated peaks were enriched for GO
554 terms associated with several non-neuronal cell types, consistent with the general hypothesis
555 that PRC functions in postmitotic cells at least in part to maintain the chosen cell fate [13] (Fig
556 6C).
557
558 To determine how EZH2 activity influences H3K27me3 distribution at early genes, we
559 created metagene plots describing H3K27me3 coverage across all H3K27me3 peaks compared
560 with the differential peaks from Fig 5D. We observed GSK-126 treatment to significantly reduce
561 H3K27me3 coverage across the 'Methylated at DIV7' cluster but not the 'Demethylated at DIV7'
562 cluster or at all H3K27me3 peaks. Visualizing H3K27me3 tracks at example early genes such as
563 *Myc* and *Gli2*, we observed GSK-126 treatment to completely block H3K27me3 compared to
564 DMSO treatment. *Grm4*, a late synaptic gene, however, remained methylated despite GSK-126
565 treatment (Fig 6D). These data argue that the function of EZH2 in postmitotic neurons over this
566 time course is to add H3K27me3 to genes that were not methylated at the time of cell fate

567 commitment. By contrast, it is not required for the maintenance of H3K27me3 at genes that
568 possessed the modification at the time of terminal differentiation, a point that we discuss below.
569
570 Finally, to determine how the gain of H3K27me3 in postmitotic CGNs affect the gene
571 expression programs that define CGN maturation, we treated CGNs with GSK-126 at either DIV1
572 or DIV3 and measured the expression of a set of early and late genes that define early and later
573 stage of CGN maturation [11, 25] (Fig 6E). CGNs treated at DIV1 still showed expression of the
574 neuronal marker gene *Tubb5,* but they showed an increase in the expression of the proliferation
575 gene *Myc*, and a striking reduction in the expression of the mature synaptic function synaptic
576 genes *Grm4* and *Grin2c,* which normally turn on at later stages of CGN maturation in culture.
577 Interestingly, when CGNs were treated with GSK-126 at DIV3, which is after the major addition
578 of H3K27me3 at GNP genes, there was no change in *Myc* expression, and there was a milder
579 reduction in *Grin2c* expression. This result suggested that EZH2 catalytic activity early on during
580 CGN maturation is critical for the silencing of early genes, which is critical for the induction of late
581 genes.

582

583 ## Discussion
584

585 In this study, we investigated the role of H3K27me3 turnover in postmitotic gene
586 regulation, using the maturation of mouse CGNs as a model system. PRC2 activity has long been
587 studied as a mechanism of early cell-fate specification in mammals through the deposition of
588 H3K27me3 and silencing of fate defining genes during the differentiation of embryonic stem cells
589 (ESCs) into other cell types including neural progenitor cells (NPCs) and early neurogenesis [5, 41,
590 42]. Our study demonstrates that dynamic changes in H3K27me3 continue in postmitotic
591 neurons at specific sites in the genome to coordinate the temporal induction of gene expression
592 programs that underlie functional maturation. Increases in H3K27me3 occurred rapidly after cell
593 cycle exit, whereas promoter demethylation occurred gradually and these turnover kinetics
594 strongly correlated with the kinetics of induced gene expression. Promoters and gene bodies that

595 gained H3K27me3 after cell cycle exit were enriched for genes involved in proliferation and cell-
596 fate specification such as *Atoh1* and *Myc*. By contrast, developmentally demethylated promoters
597 included those for genes that confer mature function on synapses such as the NMDA receptor
598 subunit *Grin2c* and the metabotropic glutamate receptor *Grm4*. This suggested to us that there
599 are temporally coordinated mechanisms of enzymatic H3K27me3 turnover during CGN
600 maturation, and that postmitotic H3K27me3 demethylation may be a key step for timing
601 functional synaptic maturation.
602
603 Our *in vivo* cerebellar data show that developmental loss of H3K27me3 from gene
604 promoters is facilitated by the H3K27me3 demethylase KDM6B, and further that conditional
605 knockout of KDM6B in CGNs impaired the expression of genes that are induced as CGNs mature.
606 *Kdm6b* expression is upregulated in newborn CGNs in the inner EGL [11], and we speculate that
607 the temporal increase in expression of this enzyme may tip the balance of H3K27me3 regulation
608 to favor histone demethylation at specific target sites. Our evidence that genes with increased
609 H3K27me3 in the *Kdm6b*-cKO mice overlap those that show developmental loss of H3K27me3 is
610 consistent with the possibility that KDM6B functions enzymatically to demethylate histones at
611 these gene promoters. However, chromatin regulators including KDM6B have scaffolding
612 functions as well as enzymatic functions [43-47], thus we attempted to use pharmacological
613 inhibition of KDM6B to validate the role of its enzymatic activity in developing CGN gene
614 regulation. The small molecule GSK-J4 is a highly selective inhibitor of the KDM6 family compared
615 with other histone demethylases, and it was previously demonstrated in primary human
616 macrophages to block LPS-mediated histone demethylation and induction of TNFα expression
617 with an IC_{50} of 9 µM and no apparent toxicity up to 30 µM [37]. By contrast we found 50%
618 cytotoxicity in CGNs at a GSK-J4 concentration of just 3.1 µM and no evidence by western blot or
619 CUT&RUN for any global or local changes in H3K27me3 when the drug was applied at the non-
620 toxic dose of 1 µM. Moving forward, as an alternative to pharmacological inhibition of KDM6B,
621 genetic mutation of the JmJC domain of KDM6B can be used to test its functional requirement in
622 neuronal H3K27me3 demethylation. Indeed, a prior study showed that in a BAC transgene,
623 enzymatically dead KDM6B was unable to rescue perinatal death in KDM6B knockout mice, which

624 is consistent with a requirement for the enzymatic function of KDM6B in maturation of the
625 respiratory circuit [48].
626
627 Our observation that H3K27me3 removal occurs at only a subset of genes that are
628 developmentally induced during CGN maturation raises the question of how these promoters are
629 marked for methylation and demethylation. Through an unbiased approach, we showed that
630 promoters that lose H3K27me3 during CGN maturation are strongly enriched for binding of the
631 transcription factors ZIC1/2; thus, one possibility is that an interaction between KDM6B and the
632 ZICs selects these genes for induction in maturing neurons. ZIC1/2 are strong drivers of CGN
633 maturation [25], and mutation of these genes is associated with cerebellar disorders, showing
634 their importance in CGN development [49, 50]. ZIC1 and 2 are zinc-finger binding proteins that
635 exhibit dynamic DNA binding properties during cerebellar maturation, and they regulate the
636 expression of both early and late CGN maturation genes [25]. Given the strong association of
637 H3K27ac enrichment at these promoters, however, it is likely that ZIC1/2 binding is a
638 consequence and not a cause of H3K27-demethylation at promoters. It would therefore be
639 essential to measure the genome-wide enrichment patterns of KDM6B during CGN maturation,
640 in order to identify its binding partners and direct targets. Existing literature investigating KDM6B
641 dynamics across the epigenome is sparse owing to the lack of well validated, commercially
642 available KDM6B antibodies. Nevertheless, KDM6B has been shown to localize to promoters and
643 enhancers of neurogenic genes in NSCs [51, 52]. KDM6B targeting to these specific loci might be
644 facilitated through interactions with TFs [52, 53], and chromatin remodeling complexes [54]. For
645 example, KDM6B has been shown to strongly associate with the ATP-dependent chromatin
646 remodeler mSWI/SNF or BAF complex, by interacting with its subunits which in turn modulate its
647 activity [55]. This interaction has been shown to play a role in neuronal development potentially
648 via H3K27me3 removal at KDM6B target sites [55, 56].
649
650 Interestingly, we find that maturation of CGN transcriptional programs not only depends
651 on the loss of H3K27me3 at genes that turn on late, but also requires the addition of H3K27me3
652 at regions that gain this mark in newly postmitotic neurons. Using CUT&RUN in cultured CGNs,

653 we discovered that the rapid increases in H3K27me3 that accumulate in newly postmitotic
654 neurons are highly sensitive to inhibition of EZH2 with GSK-126. Failure to gain H3K27me3 at
655 these sites in differentiating neurons not only prevented the developmental downregulation of
656 CGN progenitor markers like *Myc* and *Atoh1* but also impaired the developmental induction of
657 late genes like *Grm4* and *Grin2c*. The impact of GSK-126 on the mature CGN transcriptional
658 program was not due to changes in H3K27me3 regulation at the late genes themselves and was
659 more pronounced when EZH2 was inhibited immediately after cell cycle exit at DIV1 rather than
660 later at DIV3. This shows that the timing of H3K27me3 turnover is crucial in regulating the normal
661 expression of CGN-maturation genes. However, these data also raise the question of how PRC2
662 complex function can indirectly regulate the activation of late gene expression programs over a
663 period of days. One possibility is that the persistent expression of early TFs like MYC and ATOH1
664 somehow prevents the expression of the TFs that activate late gene promoters even once they
665 are demethylated. However, another possibility may be via the effects of H3K27me3 on
666 chromatin architecture. Though H3K27me3 is an acutely repressive mark, PRC2 dependent
667 deposition of H3K27me3 has been shown in some cases to contribute to physical interactions
668 between enhancers and their target genes by anchoring chromatin loops. These loops may then
669 poise genes for enhancer activation later upon receiving a developmental stimulus [57, 58]. The
670 gain of H3K27me3 in early differentiating CGNs might serve to establish such enhancer contacts
671 with the promoters of late genes. Then later when KDM6B demethylates these promoters, the
672 enhancer can permit activation. In the future, investigating dynamics in higher-order chromatin
673 structure through low-input techniques such as HiCAR [59] might help inform how H3K27me3
674 dynamics contribute to gene regulation in postmitotic neurons.

675 References

676

677 1. Hyun, K., et al., *Writing, erasing and reading histone lysine methylations.* Experimental &
678 Molecular Medicine, 2017. **49**(4): p. e324-e324.
679 2. Jambhekar, A., A. Dhall, and Y. Shi, *Roles and regulation of histone methylation in animal*
680 *development.* Nature Reviews Molecular Cell Biology, 2019. **20**(10): p. 625-641.
681 3. Daniel, J.A., M.G. Pray-Grant, and P.A. Grant, *Effector proteins for methylated histones:*
682 *an expanding family.* Cell Cycle, 2005. **4**(7): p. 919-26.

683 4. van Mierlo, G., et al., *The Complexity of PRC2 Subcomplexes.* Trends in Cell Biology, 2019.
684 **29**(8): p. 660-671.
685 5. O'Carroll, D., et al., *The polycomb-group gene Ezh2 is required for early mouse*
686 *development.* Mol Cell Biol, 2001. **21**(13): p. 4330-6.
687 6. Voncken, J.W., et al., *Rnf2 (Ring1b)*
688 *deficiency causes gastrulation arrest and cell cycle inhibition.* Proceedings of the National
689 Academy of Sciences, 2003. **100**(5): p. 2468.
690 7. Swigut, T. and J. Wysocka, *H3K27 Demethylases, at Long Last.* Cell, 2007. **131**(1): p. 29-
691 32.
692 8. Welstead, G.G., et al., *X-linked H3K27me3 demethylase Utx is required for embryonic*
693 *development in a sex-specific manner.* Proc Natl Acad Sci U S A, 2012. **109**(32): p. 13004-
694 9.
695 9. Margueron, R. and D. Reinberg, *The Polycomb complex PRC2 and its mark in life.* Nature,
696 2011. **469**(7330): p. 343-9.
697 10. Wijayatunge, R., et al., *The histone lysine demethylase Kdm6b is required for activity-*
698 *dependent preconditioning of hippocampal neuronal survival.* Mol Cell Neurosci, 2014. **61**:
699 p. 187-200.
700 11. Wijayatunge, R., et al., *The histone demethylase Kdm6b regulates a mature gene*
701 *expression program in differentiating cerebellar granule neurons.* Molecular and Cellular
702 Neuroscience, 2018. **87**: p. 4-17.
703 12. von Schimmelmann, M., et al., *Polycomb repressive complex 2 (PRC2) silences genes*
704 *responsible for neurodegeneration.* Nature Neuroscience, 2016. **19**(10): p. 1321-1330.
705 13. Ferrai, C., et al., *RNA polymerase II primes Polycomb-repressed developmental genes*
706 *throughout terminal neuronal differentiation.* Molecular Systems Biology, 2017. **13**(10):
707 p. 946.
708 14. Toskas, K., et al., *PRC2-mediated repression is essential to maintain identity and function*
709 *of differentiated dopaminergic and serotonergic neurons.* Science Advances. **8**(34): p.
710 eabo1543.
711 15. Shpargel, K.B., et al., *KDM6 demethylase independent loss of histone H3 lysine 27*
712 *trimethylation during early embryonic development.* PLoS Genet, 2014. **10**(8): p.
713 e1004507.
714 16. Maze, I., et al., *Critical Role of Histone Turnover in Neuronal Transcription and Plasticity.*
715 Neuron, 2015. **87**(1): p. 77-94.
716 17. Swahari, V. and A.E. West, *Histone demethylases in neuronal differentiation, plasticity,*
717 *and disease.* Curr Opin Neurobiol, 2019. **59**: p. 9-15.
718 18. Jepsen, K., et al., *SMRT-mediated repression of an H3K27 demethylase in progression from*
719 *neural stem cell to neuron.* Nature, 2007. **450**(7168): p. 415-9.
720 19. Burgold, T., et al., *The histone H3 lysine 27-specific demethylase Jmjd3 is required for*
721 *neural commitment.* PLoS One, 2008. **3**(8): p. e3034.
722 20. De Santa, F., et al., *Jmjd3 contributes to the control of gene expression in LPS-activated*
723 *macrophages.* Embo j, 2009. **28**(21): p. 3341-52.
724 21. Consalez, G.G., et al., *Origins, Development, and Compartmentation of the Granule Cells*
725 *of the Cerebellum.* Frontiers in Neural Circuits, 2021. **14**: p. 88.

726 22. Altman, J., *Development of the Cerebellar System.* Relation to its Evolution, Structure, and
727 Functions., 1997.
728 23. Fogarty, M.P., et al., *Fibroblast growth factor blocks Sonic hedgehog signaling in neuronal*
729 *precursors and tumor cells.* Proceedings of the National Academy of Sciences, 2007.
730 **104**(8): p. 2973-2978.
731 24. Sathyanesan, A., et al., *Emerging connections between cerebellar development, behaviour*
732 *and complex brain disorders.* Nature Reviews Neuroscience, 2019. **20**(5): p. 298-313.
733 25. Frank, C.L., et al., *Regulation of chromatin accessibility and Zic binding at enhancers in the*
734 *developing cerebellum.* Nature Neuroscience, 2015. **18**(5): p. 647-656.
735 26. Manna, S., et al., *Histone H3 Lysine 27 demethylases Jmjd3 and Utx are required for T-cell*
736 *differentiation.* Nat Commun, 2015. **6**: p. 8152.
737 27. Bilimoria, P.M. and A. Bonni, *Cultures of cerebellar granule neurons.* CSH Protoc, 2008.
738 **2008**: p. pdb.prot5107.
739 28. Suzuki, K., et al., *REAP: A two minute cell fractionation method.* BMC Research Notes,
740 2010. **3**(1): p. 294.
741 29. Love, M.I., W. Huber, and S. Anders, *Moderated estimation of fold change and dispersion*
742 *for RNA-seq data with DESeq2.* Genome Biology, 2014. **15**(12): p. 550.
743 30. Yu, G., L.-G. Wang, and Q.-Y. He, *ChIPseeker: an R/Bioconductor package for ChIP peak*
744 *annotation, comparison and visualization.* Bioinformatics, 2015. **31**(14): p. 2382-2383.
745 31. Stempor, P. and J. Ahringer, *SeqPlots - Interactive software for exploratory data analyses,*
746 *pattern discovery and visualization in genomics [version 1; peer review: 2 approved, 1*
747 *approved with reservations].* Wellcome Open Research, 2016. **1**(14).
748 32. Ashburner, M., et al., *Gene ontology: tool for the unification of biology. The Gene Ontology*
749 *Consortium.* Nat Genet, 2000. **25**(1): p. 25-9.
750 33. *The Gene Ontology resource: enriching a GOld mine.* Nucleic Acids Res, 2021. **49**(D1): p.
751 D325-d334.
752 34. Ma, M., et al., *N-myc is a key switch regulating the proliferation cycle of postnatal*
753 *cerebellar granule cell progenitors.* Scientific Reports, 2015. **5**(1): p. 12740.
754 35. Wang, Z., et al., *BART: a transcription factor prediction tool with query gene sets or*
755 *epigenomic profiles.* Bioinformatics, 2018. **34**(16): p. 2867-2869.
756 36. Wang, T.-W., et al., *Sox3 expression identifies neural progenitors in persistent neonatal*
757 *and adult mouse forebrain germinative zones.* Journal of Comparative Neurology, 2006.
758 **497**(1): p. 88-100.
759 37. Kruidenier, L., et al., *A selective jumonji H3K27 demethylase inhibitor modulates the*
760 *proinflammatory macrophage response.* Nature, 2012. **488**(7411): p. 404-408.
761 38. Lavarone, E., C.M. Barbieri, and D. Pasini, *Dissecting the role of H3K27 acetylation and*
762 *methylation in PRC2 mediated control of cellular identity.* Nature Communications, 2019.
763 **10**(1): p. 1679.
764 39. Shen, X., et al., *EZH1 mediates methylation on histone H3 lysine 27 and complements EZH2*
765 *in maintaining stem cell identity and executing pluripotency.* Mol Cell, 2008. **32**(4): p. 491-
766 502.
767 40. Chory, E.J., et al., *Nucleosome Turnover Regulates Histone Methylation Patterns over the*
768 *Genome.* Mol Cell, 2019. **73**(1): p. 61-72.e3.

41. Mohn, F., et al., *Lineage-Specific Polycomb Targets and De Novo DNA Methylation Define Restriction and Potential of Neuronal Progenitors.* Molecular Cell, 2008. **30**(6): p. 755-766.
42. Pereira, J.D., et al., *Ezh2, the histone methyltransferase of PRC2, regulates the balance between self-renewal and differentiation in the cerebral cortex.* Proceedings of the National Academy of Sciences, 2010. **107**(36): p. 15957-15962.
43. Kim, E., et al., *Phosphorylation of EZH2 activates STAT3 signaling via STAT3 methylation and promotes tumorigenicity of glioblastoma stem-like cells.* Cancer Cell, 2013. **23**(6): p. 839-52.
44. Kim, J., et al., *Polycomb- and Methylation-Independent Roles of EZH2 as a Transcription Activator.* Cell Rep, 2018. **25**(10): p. 2808-2820.e4.
45. Miller, S.A., S.E. Mohn, and A.S. Weinmann, *Jmjd3 and UTX play a demethylase-independent role in chromatin remodeling to regulate T-box family member-dependent gene expression.* Mol Cell, 2010. **40**(4): p. 594-605.
46. Xun, J., et al., *JMJD3 suppresses stem cell-like characteristics in breast cancer cells by downregulation of Oct4 independently of its demethylase activity.* Oncotarget, 2017. **8**(13): p. 21918-21929.
47. Ohguchi, H., et al., *KDM6B modulates MAPK pathway mediating multiple myeloma cell growth and survival.* Leukemia, 2017. **31**(12): p. 2661-2669.
48. Burgold, T., et al., *The H3K27 demethylase JMJD3 is required for maintenance of the embryonic respiratory neuronal network, neonatal breathing, and survival.* Cell Rep, 2012. **2**(5): p. 1244-58.
49. Twigg, S.R., et al., *Gain-of-Function Mutations in ZIC1 Are Associated with Coronal Craniosynostosis and Learning Disability.* Am J Hum Genet, 2015. **97**(3): p. 378-88.
50. Blank, M.C., et al., *Multiple developmental programs are altered by loss of Zic1 and Zic4 to cause Dandy-Walker malformation cerebellar pathogenesis.* Development, 2011. **138**(6): p. 1207-16.
51. Park, Dae H., et al., *Activation of Neuronal Gene Expression by the JMJD3 Demethylase Is Required for Postnatal and Adult Brain Neurogenesis.* Cell Reports, 2014. **8**(5): p. 1290-1299.
52. Estarás, C., et al., *Genome-wide analysis reveals that Smad3 and JMJD3 HDM co-activate the neural developmental program.* Development, 2012. **139**(15): p. 2681-2691.
53. Dai, J.P., et al., *Jmjd3 activates Mash1 gene in RA-induced neuronal differentiation of P19 cells.* J Cell Biochem, 2010. **110**(6): p. 1457-63.
54. De Santa, F., et al., *The Histone H3 Lysine-27 Demethylase Jmjd3 Links Inflammation to Inhibition of Polycomb-Mediated Gene Silencing.* Cell, 2007. **130**(6): p. 1083-1094.
55. Narayanan, R., et al., *Loss of BAF (mSWI/SNF) Complexes Causes Global Transcriptional and Chromatin State Changes in Forebrain Development.* Cell Reports, 2015. **13**(9): p. 1842-1854.
56. Nguyen, H., et al., *Epigenetic Regulation by BAF Complexes Limits Neural Stem Cell Proliferation by Suppressing Wnt Signaling in Late Embryonic Development.* Stem Cell Reports, 2018. **10**(6): p. 1734-1750.
57. Cruz-Molina, S., et al., *PRC2 Facilitates the Regulatory Topology Required for Poised Enhancer Function during Pluripotent Stem Cell Differentiation.* Cell Stem Cell, 2017. **20**(5): p. 689-705.e9.

58. Kraft, K., et al., *Polycomb-mediated genome architecture enables long-range spreading of H3K27 methylation.* Proceedings of the National Academy of Sciences, 2022. **119**(22): p. e2201883119.
59. Wei, X., et al., *HiCAR is a robust and sensitive method to analyze open-chromatin-associated genome organization.* Molecular Cell, 2022. **82**(6): p. 1225-1238.e6.

Figures and Captions

Fig 1. The maturing mouse cerebellum undergoes a genome-wide redistribution of H3K27me3 dominated by loss at promoters

A) CD1 mice were sacrificed at postnatal days 7, 14 and 60 after which cerebellar tissue was dissected out and processed to harvest histones, chromatin and RNA. B) (Left) Western blot of acid extracted histone from cerebellar tissue for H3K27me3 and total Histone H3 (n=3 biological replicates), (Right) Quantification of Western Blot, one-way ANOVA, * indicates $p < 0.05$. C) MA plot showing hypermethylated (Up) and demethylated loci (Down) throughout cerebellar maturation *in vivo* (n=3 biological replicates, differential enrichment calculated with DESeq2 package. Up and Down are loci with FDR < 0.05 and |L2FC| > 1). D) Percentage of differential H3K27me3 peaks between P7-P14, P14-P60 and P7-P60, annotated by genomic region (Annotation performed using ChIPseeker package, TSS +/- 3000 bp). E) (Left) Percentage of H3K27me3 peaks annotated by genomic region, (Right) Heatmap of H3K27me3 peaks centered around TSS +/- 3000 *bp*. F) ChIP-seq tracks of example 'Down' gene *Grin2c* (Upper) and 'Up' gene *Myc* (lower) (y-axes for ChIP-seq tracks are autoscaled according to data range in current view).

Fig 2. Differentially methylated promoters cluster by turnover kinetics and correlate with CGN maturation gene expression

A) (Left) Heatmap and hierarchical clustering of VST-transformed DESeq2-normalized counts of differential H3K27me3 promoter peaks from P7-P60, (Right) Corresponding Gene Ontology (GO) Terms associated with nearest gene and FDR. B) Violin plot showing the distribution of Log2FC of gene expression as a function of clustering performed in A, across developmental time (one-way ANOVA, * indicates $p < 0.05$). C) Example ChIP-seq tracks of genomic loci belonging to clusters

843 described in A, at *Mycn*, *Grm4* and *Grin2c* loci and corresponding RNA-seq tracks (y-axes for ChIP-
844 seq and RNA-seq tracks are autoscaled separately, according to data range in current view).
845
846 **Fig 3. *Kdm6b* knockout in CGN precursors impairs CGN maturation via H3K27me3**
847 **hypermethylation of CGN maturation gene promoters**
848 A) *Atoh1-Cre*; *Kdm6b*$^{fl/fl}$ (cKO) and *Kdm6b*$^{fl/fl}$ (WT) mice were generated by crossing *Atoh1-Cre*;
849 *Kdm6b*$^{fl/+}$ mice to *Kdm6b*$^{fl/fl}$ mice and sacrificed at P14 for cerebellar tissue harvest and
850 subsequent performing of H3K27me3 ChIP-seq (WT n=2, cKO n=3 biological replicates) and RNA-
851 seq (n=2 biological replicates). B) MA plot showing differential enrichment of genome wide
852 H3K27me3 peaks between WT and cKO mice (|Log2FC| > 1, FDR < 0.05). C) Differentially
853 methylated H3K27me3 between WT and cKO annotated by genomic location using ChIPseeker
854 package, TSS +/- 3000 bp. D) GO Terms and FDR for genes nearest genomic promoters within
855 H3K27me3 Up and Down (due to *Kdm6b*-cKO) peaks. E) Distribution of Log_2Fold Change
856 Expression (WT v cKO, computed using DESeq2) as a function of unchanged, H3K27me3 Up and
857 H3K27me3 Down genomic promoters between WT and cKO (one-way ANOVA, * indicates p <
858 0.05). F) Representative genes containing H3K27me3 Up genomic promoter peaks *Grm4* and
859 *Gabbr2* and corresponding RNA-seq tracks between WT and cKO mice (y-axes for ChIP-seq and
860 RNA-seq tracks are autoscaled separately, according to data range in current view).
861
862 **Fig 4. H3K27me3 removal is followed by gain of H3K27ac and Chromatin Accessibility at**
863 **Genomic-Promoters**
864 A) (Left) Binding Analysis for Regulation of Transcription (BART) for genes near H3K27me3 Down
865 peaks (x-axis) and near all H3K27me3 peaks (y-axis) plotted by -log_{10}p-adj. (Center) Percentage
866 of genes near H3K27me3 Down promoter peaks that are also ZIC1/2 Up (Log_2Fold Change > 1,
867 P60/P7, ZIC1/2 ChIP-seq). (Right) GO Terms and FDR for genes nearest to H3K27me3 Down
868 promoter peaks that are also ZIC1/2 Up, and not ZIC1/2 Up. B) (Left) BART analysis comparing
869 genes H3K27me3 Up peaks due to *Kdm6b*-cKO described in Fig 3. (Center) Percentage of genes
870 near H3K27me3 Up peaks due to *Kdm6b*-cKO that are also ZIC1/2 Up (Log_2Fold Change > 1,
871 P60/P7, ZIC1/2 ChIP-seq). (Right) GO Terms and FDR for genes nearest to H3K27me3 Up peaks

872 due to *Kdm6b*-cKO that are also ZIC1/2 Up, and not ZIC1/2 Up. C) Distribution of Log_2Fold Change
873 of H3K27ac enrichment and DNAse Hypersensitivity as a function of (left) H3K27me3 Gained and
874 H3K27me3 Lost described in Fig 2; and (right) Up in *Kdm6b*-cKO and Down in *Kdm6b*-cKO
875 described in Fig 3 (one-way ANOVA, * indicates $p < 0.05$). D) H3K27ac ChIP-seq and DNAse-seq
876 tracks at P7 and P60 at synaptic genes *Grm4* and *Grin2c* (y-axes for ChIP-seq and DNAse-seq
877 tracks are autoscaled separately, according to data range in current view).
878
879 **Fig 5. CGN Culture System Preserves Dynamic Changes in H3K27me3 at Promoters**
880 A) Schematic describing CGN culture protocol over 7 days *in vitro* annotated with early and late
881 CGN genes. B) Differentially methylated H3K27me3 CUT&RUN peaks annotated by genomic
882 location, between DIV1-3, 3-5, 5-7 and 1-7 time points. C) Percentage of differential H3K27me3
883 CUT&RUN peaks between DIV1-3, DIV3-5, DIV5-7 and DIV1-7 annotated by genomic region
884 (Annotation performed using ChIPseeker package, TSS +/- 3000 bp). D) (Left) Heatmap and
885 hierarchical clustering of VST-transformed DESeq2-normalized counts of differential H3K27me3
886 CUT&RUN promoter peaks from DIV1-7 (Right) Corresponding GO Terms and FDR associated with
887 nearest gene. E) CUT&RUN tracks for H3K27me3 for (top) late genes *Grin2c*, and *Grm4* and
888 (bottom) *Myc* and *Atoh1* at DIV1, 3, 5 and 7 (y-axes for CUT&RUN tracks are autoscaled according
889 to data range in current view). F) Violin plot showing the distribution of Log2FC of gene
890 expression between DIV0 and DIV7 CGNs as a function of clustering performed in E (one-way
891 ANOVA, * indicates $p < 0.05$).
892
893 **Fig 6. EZH2 catalytic activity temporally regulates CGN maturation in culture by depositing**
894 **H3K27me3 at early CGN genes**
895 A) (Left) Western blot of acid extracted histones from CGNs treated for H3K27me3 and total
896 Histone H3 (n=3 biological replicates). CGNs were treated with GSK-J4 or GSK-126 at DIV1 and
897 harvested at DIV5, (Right) Quantification of Western blot. B) MA plot describing differential
898 methylation due to GSK126 treatment in cultured CGNs (FDR < 0.05 and |L2FC| > 1) (n=3
899 biological replicates). C) Metagene plots for H3K27me3 peaks of DMSO and GSK-126 treated
900 CGNs at (left) All H3K27me3 peaks, and (center) peaks methylated at DIV7, (right) demethylated

901 at DIV7, described in Fig 5E. D) Representative CUT&RUN tracks for early genes *Myc* (left) and
902 *Gli2* (center) and synaptic gene *Grm4*, for DMSO and GSK126 treated CGNs (y-axes for CUT&RUN
903 tracks are autoscaled according to data range in current view). E) RT-qPCR for early genes *Tubb5*,
904 *Myc* and *Gli2*, and synaptic genes *Grm4* and *Grin2c* due to GSK126 treatment at DIV1 (left) and
905 DIV3 (right) (n=3 biological replicates, one-way ANOVA, * indicates $p < 0.05$)
906
907
908
909
910

Figure 1. The maturing mouse cerebellum undergoes a genome-wide redistribution of H3K27me3 dominated by loss at promoters

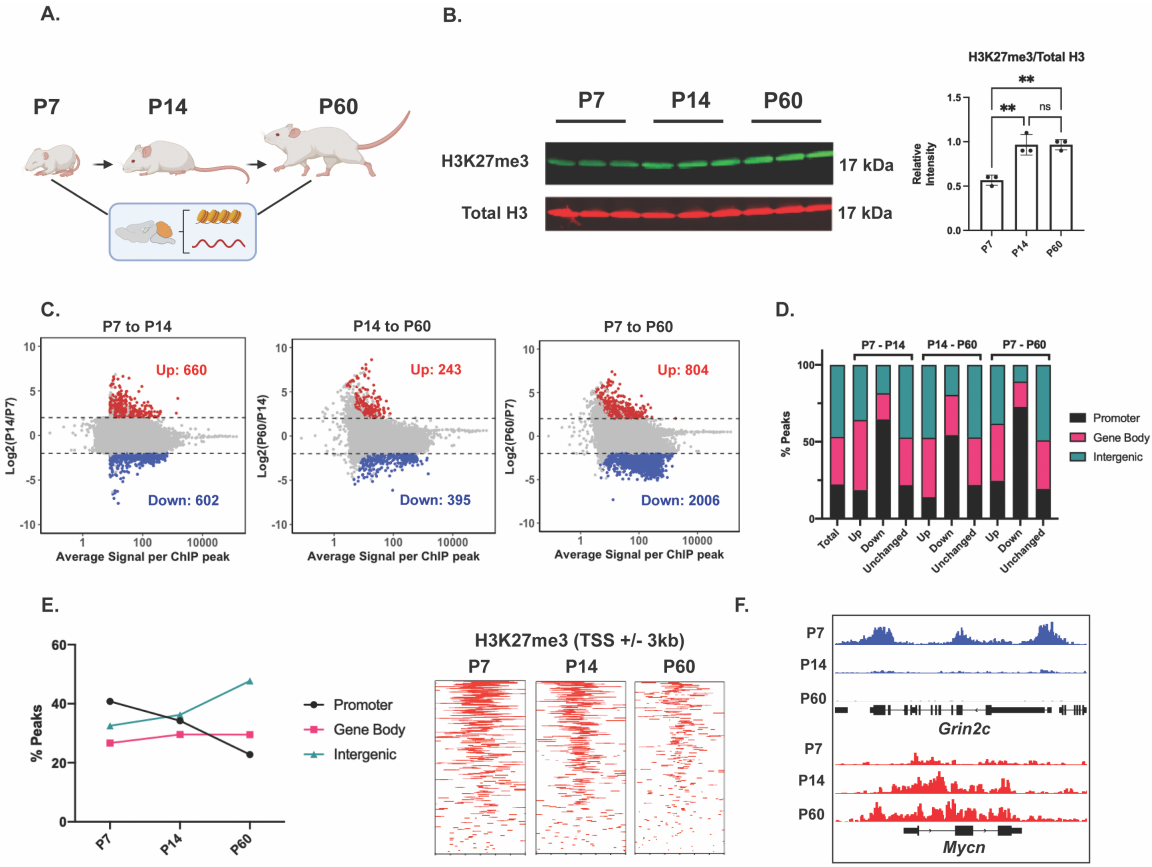

Figure 2. Differentially methylated promoters cluster by turnover kinetics and correlate with CGN maturation gene expression

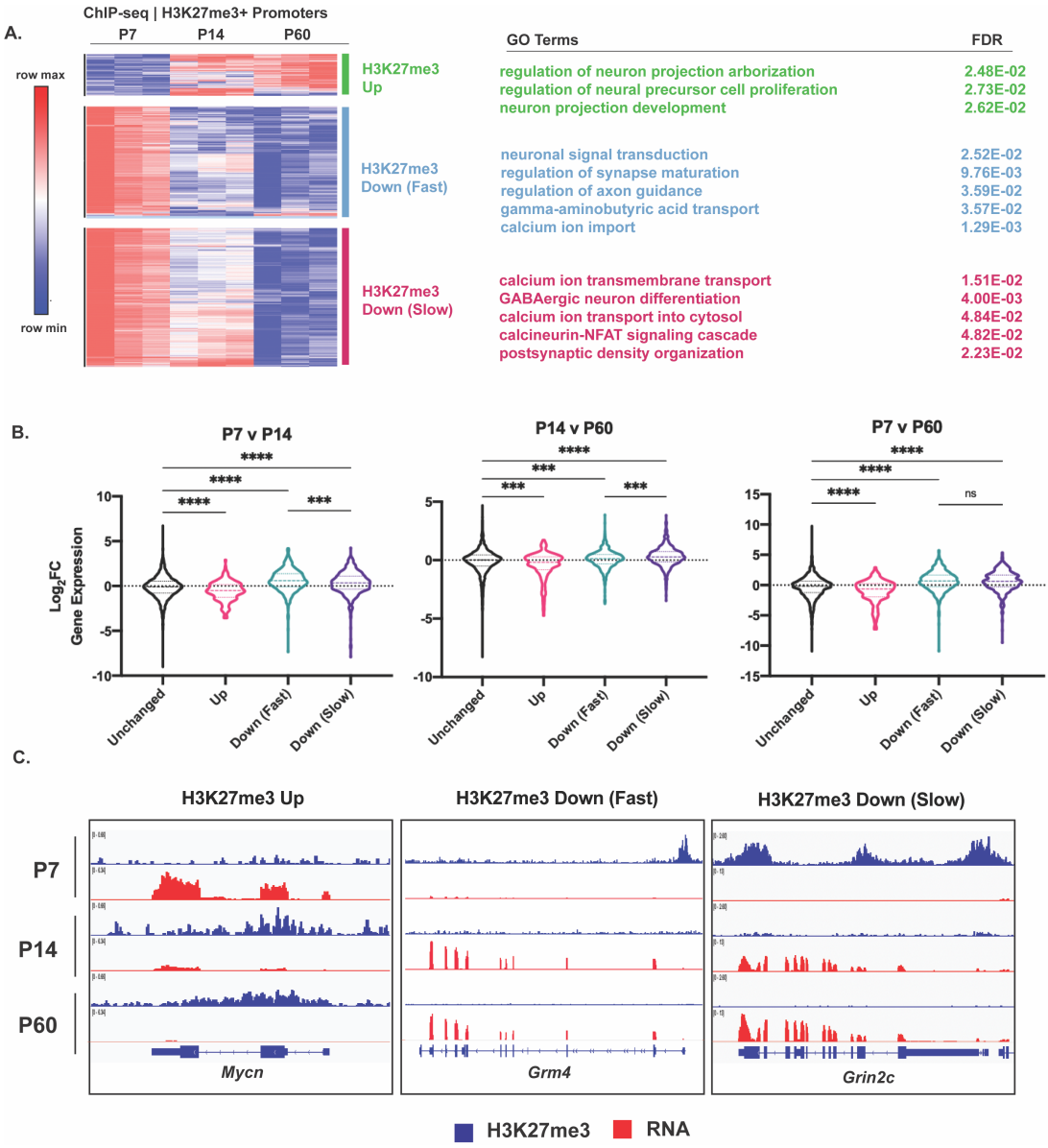

Figure 3. *Kdm6b* knockout in CGN precursors impairs CGN maturation via hypermethylation of CGN maturation gene promoters

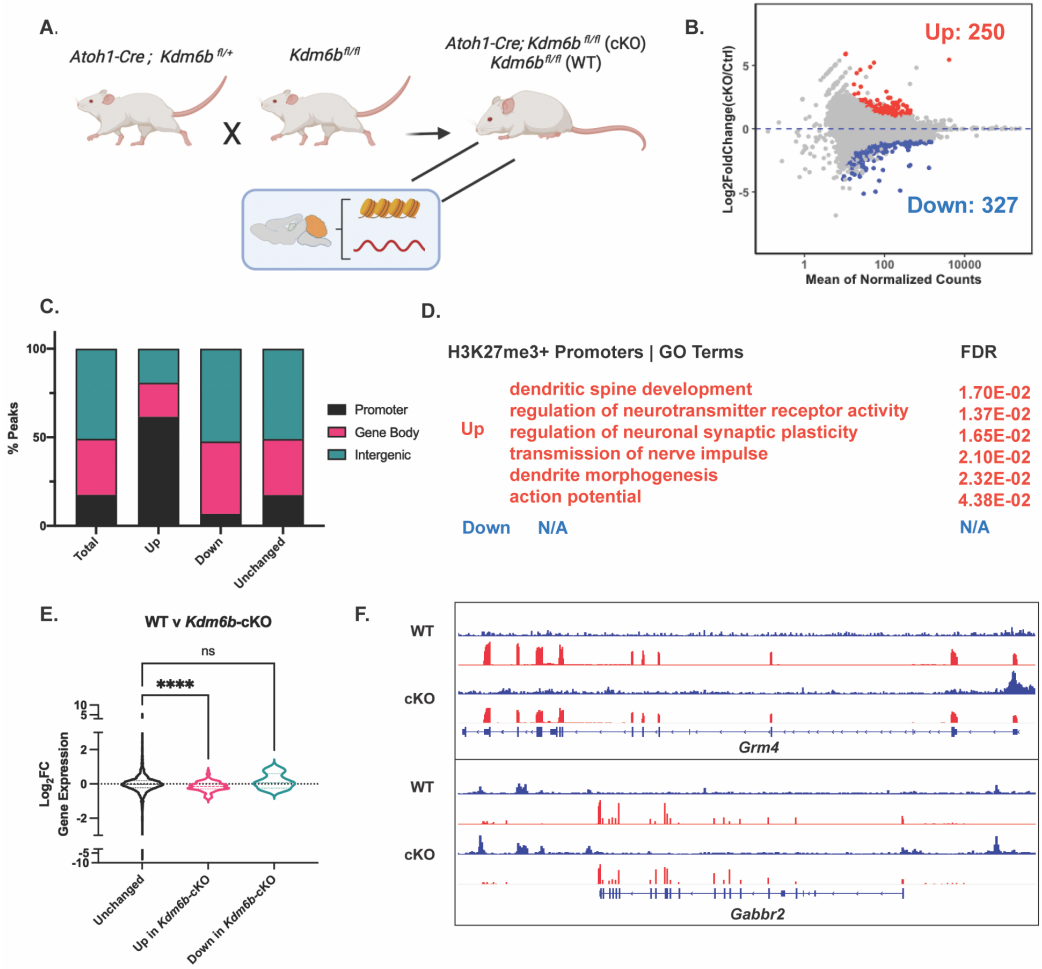

Figure 4. H3K27me3 Removal is Characterized by Gain of H3K27ac and Chromatin Accessibility at Genomic-Promoters

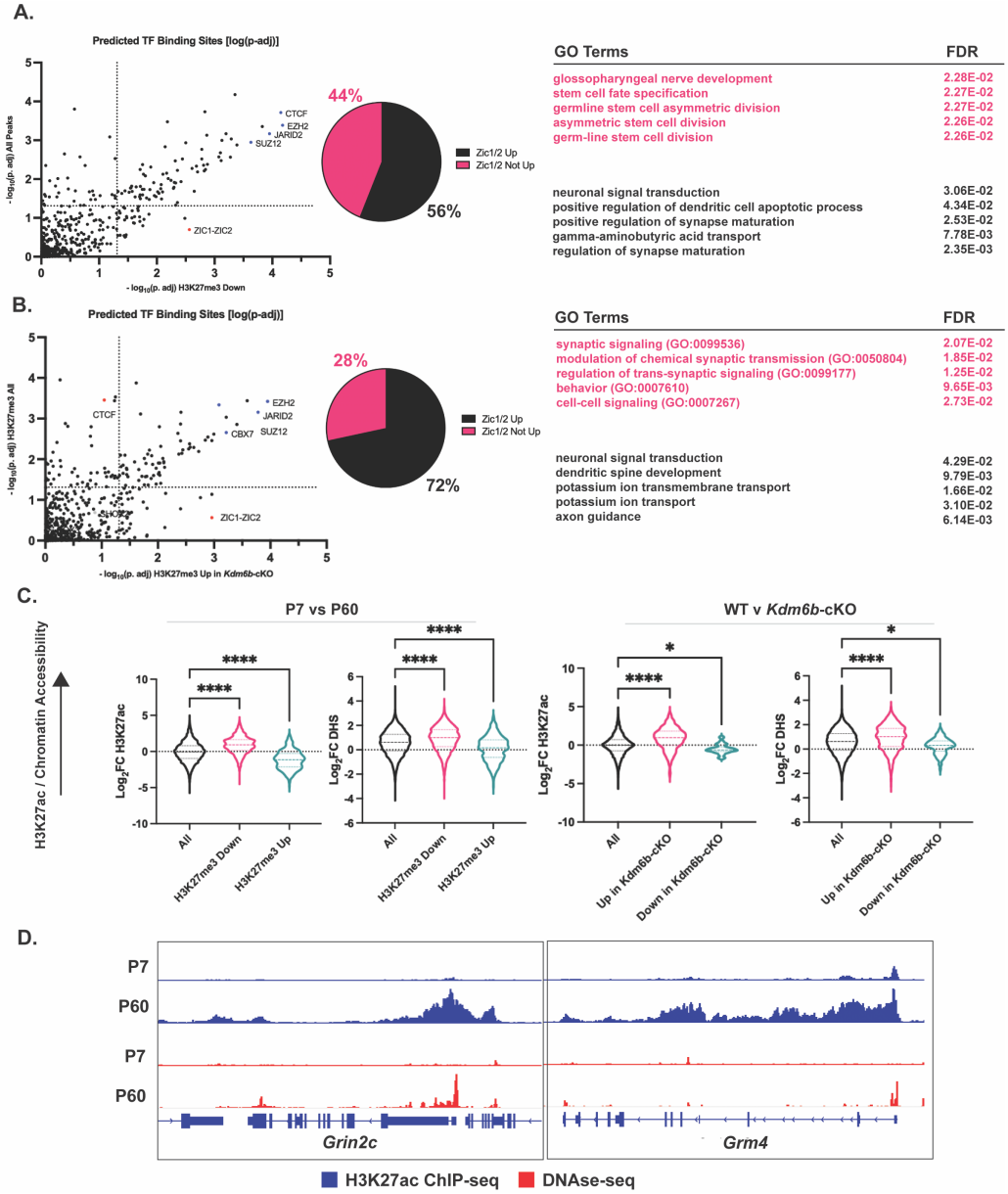

Figure 5. CGN Culture System Preserves Dynamic Changes in H3K27me3 at Promoters

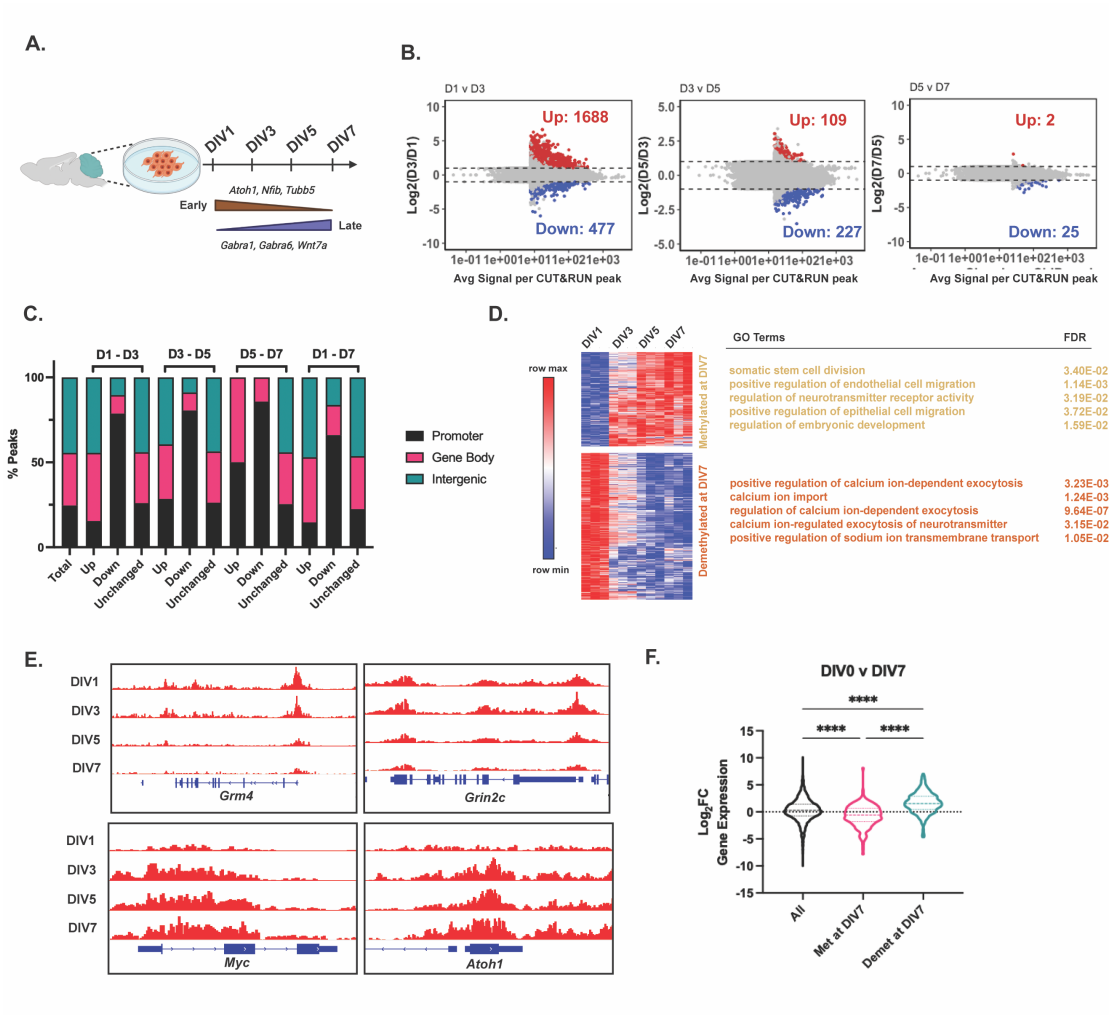
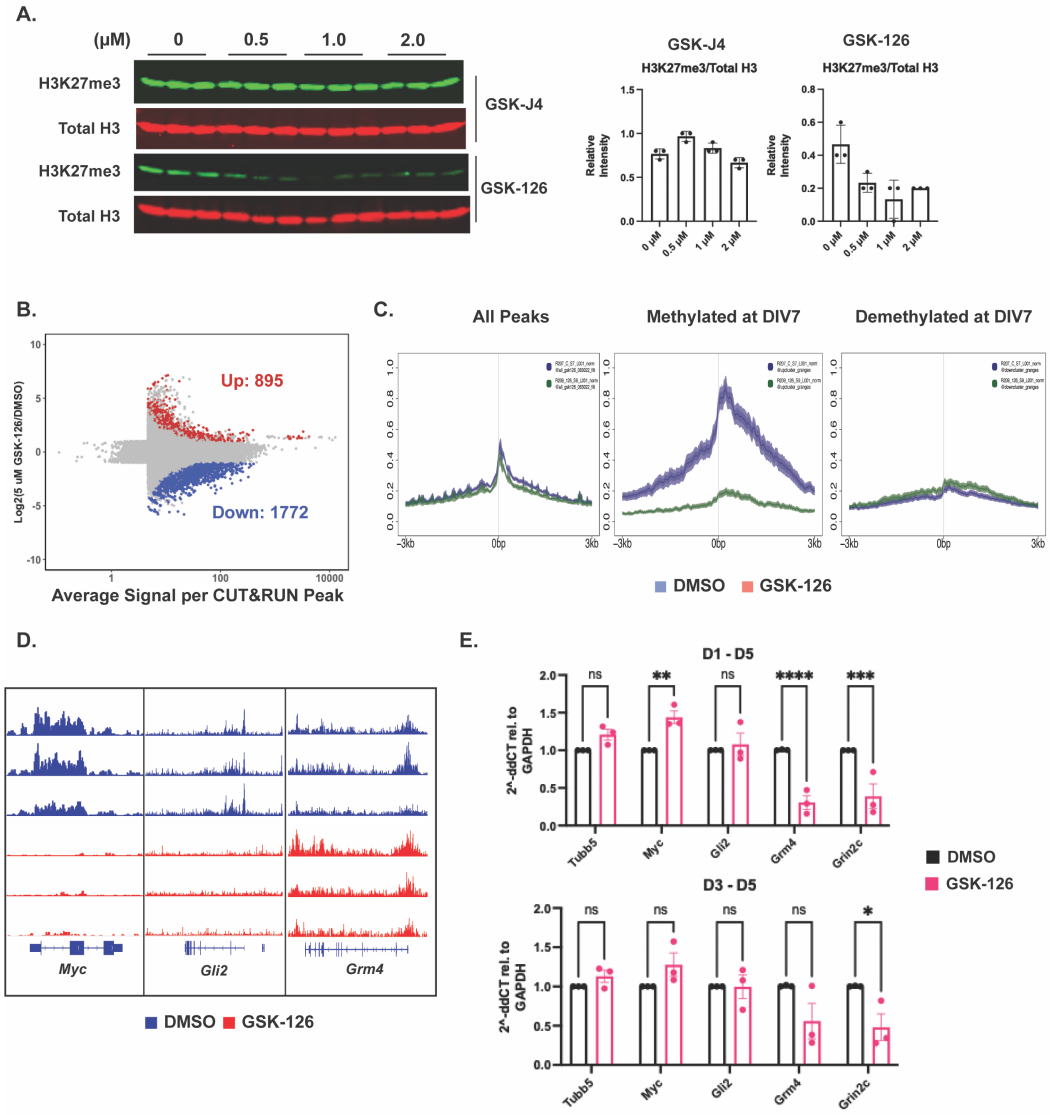
Figure 6. EZH2 catalytic activity temporally regulates CGN maturation in culture